Constellation Design Enhancement for Color-Shift Keying Modulation of Quadrichromatic LEDs in Visible Light Communications

Xiao Liang, *Member, IEEE*, Ming Yuan, Jiaheng Wang, *Senior Member, IEEE*, Zhi Ding, *Fellow, IEEE*, Ming Jiang, *Member, IEEE*, and Chunming Zhao, *Member, IEEE*

***Abstract*—Quadrichromatic light-emitting diode (QLED) cluster is a four-color solid-state apparatus suitable for simultaneous illumination and communications. Unlike traditional red/green/blue (RGB) LEDs, its extra color provides not only one new wavelength-division multiplexing data channel but also better color quality in illumination. Taking full consideration of the high quality of color rendering index (CRI) requirement with tunable color temperature (CT), this paper investigates the constellation design of color shift keying (CSK) to maximize the minimum pairwise Euclidean distance (MED) for communication performance optimization. Beyond existing works, maintaining a high-level CRI with a specified CT complicates our design optimization problem. We propose to transform the CRI requirement into a set of linear constraints on one of the LED source composition while jointly incorporating the CT constraints. Both simulation results and prototype CSK communication testbed measurements based on commercial multicolor LEDs (LUMILEDS Luxeon C) illustrate that, under the same luminous flux and CT conditions, our proposed flux independent CSK constellation for QLEDs can significantly enhance the MED, bit error rate, and illumination color qualities.**

***Index Terms*—Color rendering index, color shift keying, color temperature, minimum Euclidean distance, quadrichromatic LED cluster, visible light communications.**

I. Introduction

HIGHLY bright light-emitting diodes (LEDs) are rapidly replacing conventional lighting devices due to low cost, long life and high power efficiency [1]. Meanwhile LED's fast switching capability also stimulates substantial research interest in its use for visible light communications (VLC) [2]. Through wavelength division multiplexing (WDM), VLC transceiver with multi-color LED naturally forms a color-space multiple input and multiple output (CMIMO) channels, which in turn can achieve multi-fold increase in channel capacity [3]–[5] when compared with single-color channel [6].

We focus on the use of color shift keying (CSK) modulation, which is originally proposed in IEEE 802.15.7 [7] for transceiver with red/green/blue (RGB) LEDs. LED is an unipolar device with limited dynamic range [8]. Usually, driving such device with high PAPR signal would lead to severe nonlinear distortion and clipping noises [9], [10]. Since CSK could be viewed as a single carrier (SC) WDM modulation, CSK modulation exhibits much lower peak-to-average ratio (PAPR) than discrete multitone or orthogonal frequency-division multiplexing (DMT/OFDM) WDM modulation. Moreover, a carefully designed CSK constellation could mitigate the effect of nonlinear distortion. The transceiver design for CSK VLC is also simpler and less costly compared with DMT/OFDM WDM systems. Furthermore, since CSK can maintain a steady instantaneous luminance across each constellation, CSK-based VLC advantageously prevents intensity flicker and reduces potential inrush of device current.

The design of CSK constellation for RGB LEDs has been widely investigated. In [11] and [12], billiards algorithms and interior point methods, respectively, were utilized for designing CSK constellations. In [13], the authors have demonstrated a CSK VLC prototype with optimized constellation design for RGB LEDs, delivering a gain of 1-3 dB over standard 802.15.7 constellations. The authors in [14] presented a novel design by jointly taking advantage of color and frequency domains with adaptive DC-bias on RGB LED-based communication systems. Authors in [15] also combined CSK with pulse position modulation (PPM) to improve efficiency.

Note that, in lighting technology, to improve the color qualities of white illumination light, quadrichromatic LEDs (QLED), usually with red/green/blue/amber (RGBA) colors, have been suggested as alternative to RGB LEDs [16]. Several works [17], [18] have already revealed the tradeoff between CRI and luminous efficacy of white lights synthesized by no more than five primary colors. Further, the work in [19] utilized

Manuscript received September 7, 2016; revised January 16, 2017 and June 17, 2017; accepted June 20, 2017. Date of publication June 26, 2017; date of current version July 11, 2017. This work was supported in part by the 973 Program under Grant 2013CB329204, by the National Natural Science Foundation of China under Grants 61571107, 61601115, 61521061, and 61461136003, by the Natural Science Foundation of Jiangsu Province under Grant BK20160069, and by the Alexander von Humboldt Foundation. The work of Z. Ding was supported by the National Science Foundation under Grants CNS-1702752 and CCF-1443870. *(Corresponding author: Xiao Liang.)*

X. Liang, M. Yuan, J. Wang, M. Jiang, and C. Zhao are with the National Mobile Communications Research Laboratory, Southeast University, Nanjing 210096, China (e-mail: xiaoliang@seu.edu.com; yuanming@seu.edu.cn; jhwang@seu.edu.cn; jiang_ming@seu.edu.cn; cmzhao@seu.edu.cn).

Z. Ding is with the Department of Electrical and Computer Engineering, University of California, Davis, CA 95616 USA, and also with the National Mobile Communications Research Laboratory, Southeast University, Nanjing 210096, China (e-mail: zding@ucdavis.edu).

Color versions of one or more of the figures in this paper are available online at http://ieeexplore.ieee.org.

Digital Object Identifier 10.1109/JLT.2017.2720579

commercial multi-color LEDs to synthesize white lights. Meanwhile, with its extra wavelength in QLED, VLC performances are expected to improve significantly. For example, the work in [20] demonstrated 5.6-Gbps downlink data rate with DMT modulation using QLED. Also, the work in [5] updated the data rate to 8-Gbps by employing high-order CAP modulation and hybrid post equalizer.

In this work, we will focus on CSK constellation design for QLEDs. Several related works have already appeared. In [21], metameric modulation is proposed by using $D > 3$ wavelength LEDs to transmit multiple lighting states that are indistinguishable to human perception of illumination but are distinguishable to photo detectors (PD). In [10], an enhanced CSK modulation scheme using QLED is proposed and the CSK constellations were designed directly on the chromaticity diagram.

We note that it is possible to simply extend the constellation design approaches used for RGB LEDs for QLEDs [22]. Nevertheless, such naïve approaches fail to address the important question regarding how to jointly maximize the MED of constellation for communication quality while maintaining the high color quality for illumination. In particular, the color rendering index (CRI) of white light generated by QLED should be considered for optimization. In fact by Grassmann's law [23], when the number of wavelength is greater than three, we now have a set of feasible operating points instead of only one point to map to a specified color temperature (CT). Hence, we will choose the best CSK constellation among these operating points for QLEDs. On the other hand, integration of the CRI constraint in CSK design can substantially complicate the design complexity [24], since the existing formulations of CSK design for RGB LEDs could not directly accommodate the complex CRI constraint. For the aforementioned reasons, few works have studied this design problem. In this work, our major contributions lie in the design optimization of CSK constellations under the physical constraint of tunable color temperature, flexible luminous flux, as well as the guarantee of high color quality of CRI.

In Section II, we provide essential background information on the basics of illumination lighting. We formulate the design problem by establishing the CMIMO channel model. In Section III, we first reformulate the CT and CRI constraints for QLED to a set of linear constraints with disjoint convex sets. We then utilize iterative method to obtain the optimized constellations. Section IV will present both comprehensive numerical and experimental performance comparisons between commercial QLEDs and RGB LEDs before concluding in Section V.

II. Problem Formulation for CSK Constellation Design With QLED

In this section, we first briefly review some basic information with respect to illumination engineering. We will investigate the multi-color VLC channel model before presenting the design problem formulation,

A. Metamerism and Color Rendering Index

Assume the spectral power distribution (SPD) of a light is $\varphi(\lambda)$. Human visual response of $\varphi(\lambda)$ can be described in terms

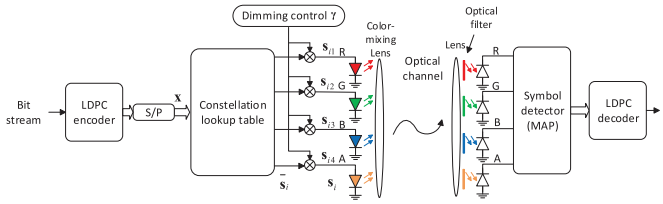

Fig. 1. Multi-color CSK transceiver with QLED cluster.

of tri-stimulus values vector $\mathbf{a}_\varphi$ in CIE XYZ color space [25], which are given as

$$\mathbf{a}_\varphi = \begin{bmatrix} \int \varphi(\lambda)\bar{x}(\lambda)d\lambda \\ \int \varphi(\lambda)\bar{y}(\lambda)d\lambda \\ \int \varphi(\lambda)\bar{z}(\lambda)d\lambda \end{bmatrix} = \frac{\mathcal{L}}{683} \begin{bmatrix} \frac{x_\varphi}{y_\varphi} \\ 1 \\ \frac{1-x_\varphi-y_\varphi}{y_\varphi} \end{bmatrix} \tag{1}$$

where $\bar{x}(\lambda)$, $\bar{y}(\lambda)$ and $\bar{z}(\lambda)$ are color matching functions for red, green and blue primary colors, respectively. On the other hand, point in CIE XYZ color space can also be translated to CIE XYY color space, where (x_φ, y_φ) is the corresponding coordinate and $\mathcal{L}$ is the luminous flux.

The temperature of an ideal blackbody radiator is defined as the color temperature. To generate the white light associated with a specified CT, the color coordinates of the white light must be matched to that point $\mathbf{a}_{\text{CT}}$ on blackbody curve on the chromaticity diagram.

Consider the case for which there are L primary-color LEDs. Driven by the maximal permitted current of each color LED chip, the SPD of l-th primary color is $\varphi_l(\lambda)$. The collection of tri-stimulus values vector of $\varphi_l(\lambda)$ $(l = 1, \ldots, L)$ is a 3-by-L matrix $\mathbf{A}_{tv}$, e.g., the l-th column is the tri-stimulus values vector of $\varphi_l(\lambda)$. Assuming the following color matching equations are feasible

$$\begin{cases} \mathbf{A}_{tv}\mathbf{i} = \mathbf{a}_{\text{CT}} \\ \mathbf{0} \preceq \mathbf{i} \preceq \mathbf{1} \end{cases} \tag{2}$$

we can obtain a percentage of luminous flux vector $\mathbf{i} = [i_1, \ldots, i_L]^T$ for L primary-color LEDs, which synthesizes the same apparent color $\mathbf{a}_{\text{CT}}$.

On the other hand, the effect of metamerism indicates that the reverse mapping from color coordinates $\mathbf{a}_{\text{CT}}$ to SPD is generally not unique, which means that lights with different relative SPDs could have the same apparent color. However, qualities of those lights are generally not the same. Color rendering index is a quantitative measure of the ability of an illumination source to faithfully reveal the colors of various objects in comparison with an ideal or natural light source. CRI is the function of illumination SPD, and the procedure of CRI calculation is rather complex [24]. In this paper, we will refer the general color rendering index R_a to CRI.

Note that, when the number of primary color $L > 3$, the solution of (2) is not unique. This is why our proposed QLED device has the ability to tune R_a while maintaining a specified CT.

B. CMIMO Channel Model With QLED

Fig. 1 illustrates a typical CSK transceiver. For a multi-color LED based white light VLC system, color-mixing lens are necessary to provide good color uniformity with high luminous output. The front end of multi-color receiver comprises photodetectors (PD), low-noise amplifiers, and the associated optical filters. Due to the non-ideal bandpass and the partial overlap of wavelength of emitted colors, the optical channel actually can be described as a 4-by-4 color-space multiple inputs and multiple outputs channels $\mathbf{H}$.

Let ϕ be the angle of irradiance of QLED and ψ be the angle of incidence of multi-color receiver, respectively. Then, $T(\phi)$ is the gain of color mixing lens and $L(\psi)$ is the gain of optical lens. Let A be the receiving area of the PD receiver, Ψ be the multi-color receiver's field of view (FOV), and d denote the distance between QLED and multi-color receiver, respectively. The order of Lambertian emission is given by

$$m = -\frac{\ln 2}{\ln(\cos \Phi_{1/2})}$$

where $\Phi_{1/2}$ is the semi-angle at half optical power of LED. Furthermore, suppose $F_i(\psi, \lambda)$ is the gain of i-th color filter with respect to incidence angle ψ and wavelength λ, $\bar{\varphi}_j(\lambda)$ is the SPD of j-th color LED driven by the maximal permitted current, $R_o(\lambda)$ is the intrinsic responsivity of PD receiver at wavelength λ.

Therefore, when $0 \le \psi \le \Psi$, the element of $\mathbf{H}$ induced by j-th incident color through i-th color receiver [1] is

$$\begin{aligned}[\mathbf{H}]_{ij} = \ & \tfrac{(m+1)A}{2\pi d^2} \cos^m(\phi) T(\phi) L(\psi) \cos(\psi) \\ & \cdot \textstyle\int_{380}^{780} \bar{\varphi}_j(\lambda) F_i(\psi, \lambda) R_o(\lambda) d\lambda \end{aligned} \tag{3}$$

otherwise $[\mathbf{H}]_{ij} = 0$.

C. Problem Formulation

As shown in Fig. 1, binary data are converted to N-by-1 vector $\mathbf{x}$ for transmission. Then $\mathbf{x}$ is mapped to one of 4-by-1 QLED CSK constellations $\bar{\mathbf{s}}_i$ (the constellation optimized at some luminous flux), where $i \in \{1, \ldots, M = 2^N\}$. To meet the dimming requirement, the percentage of luminous flux vector $\mathbf{s}_i$ eventually controls the QLED driver, which is obtained by multiplying $\bar{\mathbf{s}}_i$ to a common dimming factor $\gamma \ge 0$ as in

$$\begin{aligned} \mathbf{s}_i &= \gamma \bar{\mathbf{s}}_i \\ \text{where } \mathbf{0} &\preceq \mathbf{s}_i \preceq \mathbf{1}_4 \end{aligned} \tag{4}$$

where $\mathbf{1}_M$ denotes a M-length all one column vector.

Let $\mathbf{I}_4$ be the 4×4 identity matrix and let $\otimes$ denote the Kronecker product. Since all constellation points $\{\mathbf{s}_i\}$ are equiprobable, the constellation centroid (the average of constellation points) can be written as $\frac{1}{M}\mathbf{C}\mathbf{s}$, where $\mathbf{s} = \left[\mathbf{s}_1^T, \ldots, \mathbf{s}_M^T\right]^T$, and $\mathbf{C} = \mathbf{1}_M^T \otimes \mathbf{I}_4$. Despite the unique color of each constellation $\mathbf{s}_i$, as long as the data rate is high enough, the apparent color of illumination is determined by the constellation centroid. Therefore, in light of the color matching requirement (2), the tri-stimulus values vector of the apparent light $\mathbf{a}_{\text{CT}}$ is linked with the constellation centroid in the form of

$$\frac{1}{M}\mathbf{A}_{tv}\mathbf{C}\mathbf{s} = \mathbf{a}_{\text{CT}} \ . \tag{5}$$

Note that despite the luminous constraint on the average constellation in (6), CSK design requires that each constellation also has a constant luminance to prevent potential flicking in illumination. Specifically, these requirements can be captured by

$$\left(\mathbf{I}_M \otimes [\mathbf{A}_{\text{tv}}]_{2,:}\right)\mathbf{s} = \frac{\mathcal{L}}{683} \cdot \mathbf{1}_M \tag{6}$$

where $\mathcal{L}$ is the target luminance flux, and $[\mathbf{A}_{\text{tv}}]_{i,:}$ denotes the i-th row of matrix $\mathbf{A}_{\text{tv}}$ in (2).

As we know, the minimum pairwise Euclidean distance (MED) of symbols in the received signal space is quite different than that in color space, especially when the MED is distorted by CMIMO channels. Works by [10], [25] indicate that intensity detection could achieve much better performance over chromaticity detection. Therefore, in this work, we shall focus on the MED of symbols in received signal space.

Following [14], the difference between received i-th and j-th constellations can be expressed in the following compact form

$$\underbrace{\left((\mathbf{e}_i - \mathbf{e}_j) \otimes \mathbf{I}_4\right)^T \left(\mathbf{I}_M \otimes \mathbf{H}\right)}_{\mathbf{E}_{ij}}\mathbf{s} \tag{7}$$

where $\mathbf{e}_i$ is the i-th column of $\mathbf{I}_M$.

Finally, combining conditions in (4)–(7), the CSK constellation design could be formulated as

$$\max_{\mathbf{s}} \quad d_{\min} \tag{8a}$$

$$\text{s.t.} \quad \mathbf{s}^T \mathbf{E}_{ij}^T \mathbf{E}_{ij} \mathbf{s} \ge d_{\min}^2 \ , \ 1 \le i < j \le M \tag{8b}$$

$$\text{CT:} \quad \frac{1}{M}\mathbf{A}_{tv}\mathbf{C}\mathbf{s} = \mathbf{a}_{\text{CT}} \tag{8c}$$

$$\text{Luminance:} \quad \left(\mathbf{I}_M \otimes [\mathbf{A}_{\text{tv}}]_{2,:}\right)\mathbf{s} = \frac{\mathcal{L}}{683} \cdot \mathbf{1}_M \tag{8d}$$

$$\text{CRI:} \quad R_a \ge \beta \tag{8e}$$

$$\text{Amplitude:} \quad \mathbf{0} \preceq \mathbf{s} \preceq \mathbf{1} \tag{8f}$$

where β is the feasible target CRI value.

Clearly, the constraints in (8b) are non-convex. Furthermore, according to [24], since the CRI evaluation is very complicated, the region defined by (8e) is also generally non-convex. Therefore the problem in (8a)–(8f) is non-convex and difficult to solve efficiently. In the next section, we will try to overcome these difficulties one-by-one.

III. CSK Constellation Design

In this section, we firstly numerically transform the complicated CRI constraint into linear constraints with a set of disjoint convex regions by jointly considering the CT constraint. We

[1] Since both QLED cluster and multi-color receiver are assumed to be assembled in a compact package, and the distance between transmitter and multi-color receiver is much larger than either the physical size of QLED cluster or multi-color receiver, both QLED cluster and multi-color receiver could be viewed as points, respectively.

then adopt the method proposed in [26] to iteratively obtain the optimized constellations.

A. Reformulation of Lighting Constraints: CT and CRI

Observe the CT constraints (2). Since the tri-stimulus value matrix $\mathbf{A}_{\text{tv}}$ is 3-by-4, the solution for $\mathbf{i}$ falls in a one dimension space. Without loss of generality, partition vector $\mathbf{i}$ and matrix $\mathbf{A}_{\text{tv}}$ as follows

$$\mathbf{i} = \begin{bmatrix} \mathbf{i_{1:3}} \\ i_4 \end{bmatrix}, \ \mathbf{A}_{\text{tv}} = \begin{bmatrix} \mathbf{A_{1:3}} \ \mathbf{a}_4 \end{bmatrix}$$

where $\mathbf{i}_{1:3}$ is the first three elements of vector $\mathbf{i}$, and $\mathbf{A}_{1:3}$ is the first three columns of $\mathbf{A}_{\text{tv}}$. Substituting these partitions into (2), we can obtain the solution of CT constraint in (2) as

$$\mathbf{i} = \alpha \cdot \underbrace{\begin{bmatrix} -\mathbf{A}_{1:3}^{-1} \cdot \mathbf{a}_4 \\ 1 \end{bmatrix}}_{\mathbf{c}_1} + \underbrace{\begin{bmatrix} \mathbf{A_{1:3}^{-1}} \cdot \mathbf{a}_{\text{CT}} \\ 0 \end{bmatrix}}_{\mathbf{c}_2} \tag{9}$$

where α is the freedom scalar which may assume any value so long as $\mathbf{1} \succeq \mathbf{i} \succeq 0$.

Following [24], the color rendering index R_a is determined by the illumination light SPD, which is shaped by the percentage of luminous flux vector $\mathbf{i}$ for multi-color based illumination systems. Consequently, R_a is also a function of α in (9). Hence, the CRI constraint in (8e) is equivalent to finding the feasible region of α to qualify the minimum R_a requirement,

$$\begin{array}{c} \{\alpha | \alpha \in [0,1], R_a(\alpha) > \beta\} \\ \Downarrow \\ \alpha \in [\alpha_1, \alpha_2] \cup [\alpha_3, \alpha_4] \cup \cdots \cup [\alpha_{2L_\alpha - 1}, \alpha_{2L_\alpha}] \end{array} \tag{10}$$

where we let $0 \le \alpha_1 \le \alpha_2 \le \cdots \le \alpha_{2L_\alpha} \le 1$. Generally, as shown in (10), the feasible region of α comprises L_α disjoint regions. However CRI constraint does not admit an analytical approach to obtain the feasible region of α. Instead, we can resort to numerical means for determining the feasible region of α. Several numerical examples will be elaborated in Section IV-B.

Finally, we have equivalently converted the constraints (11) and (13) to

$$\begin{cases} \frac{1}{M}\mathbf{C}\mathbf{s} = \alpha \mathbf{c}_1 + \mathbf{c}_2 \\ \alpha \in [\alpha_1, \alpha_2] \ \cup \cdots \cup \ [\alpha_{2L_\alpha - 1}, \alpha_{2L_\alpha}] \end{cases} \tag{11}$$

where $\mathbf{c}_1 = [c_{11}, c_{12}, c_{13}, 1]^T$ and $\mathbf{c}_2 = [c_{21}, c_{22}, c_{23}, 0]^T$ are defined in (15), and $\alpha_1, \alpha_2, \cdots, \alpha_{2L_\alpha}$ are defined in (10). Clearly, for each connected interval of $\alpha \in \mathcal{C}_i$ where $\mathcal{C}_i = [\alpha_{2i-1}, \ \alpha_{2i}], \ i = 1, 2, \cdots, \ L_\alpha$, the constraint

$$\begin{cases} \frac{1}{M}\mathbf{C}\mathbf{s} = \alpha \mathbf{c}_1 + \mathbf{c}_2 \\ \alpha \in \mathcal{C}_i \end{cases}$$

is linear and convex.

B. Iterative CSK Constellation Optimization

Remember that, since the constraints in (8b) are non-convex, the problem defined in (8a)–(8f) is still NP-hard. To overcome this difficulty, we adopt the method in [26].

Suppose that we have a feasible solution $\mathbf{s}_{(0)}$. The quadratic constraints in (8b) could be linearly lower-bounded as follows

$$2\mathbf{s}_{(0)}^T \mathbf{E}_{ij}^T \mathbf{E}_{ij} \mathbf{s} - \mathbf{s}_{(0)}^T \mathbf{E}_{ij}^T \mathbf{E}_{ij} \mathbf{s}_{(0)} \ge d_{\min}^2 . \tag{12}$$

Therefore, combined with (11) and considering one subregion $\alpha \in \mathcal{C}_i, i = 1, \ldots, \ L_\alpha$, the original optimization problem can be approximated by a convex one that could be solved efficiently, e.g., by CVX.[2] Since the optimal solution $\mathbf{s}$ and $d_{\min}$ of convex problem are in fact suboptimal for the original problem (8a)–(8f), we can run the program based on multiple (e.g., 500) random selections of feasible solution $\mathbf{s}_{(0)}$ and choose the best one as the result for subregion $\mathcal{C}_i$. The process is repeated for every subregion of $\alpha \in \mathcal{C}_i, \ i = 1, \ldots, L_\alpha$, before selecting the best result as the final solution $\mathbf{s}^*$ and $d_{\min}^*$.

(*Algorithm* Iterative CSK Constellation Optimization).

1: $d_{\min}^* = 0$
2: **for** $l = 1$ to L_α **do**
3: *Initialization* : $\alpha \in \mathcal{C}_l$
4: **for** $m = 1$ to 500 **do**
5: Generate initial feasible solution $\mathbf{s}_{(0)}$ randomly.
6: Solve the following convex problem:

$$\begin{array}{ll} \max\limits_{\mathbf{s}} & d_{\min} \\ \text{s.t.} & 2\mathbf{s}_{(0)}^T \mathbf{E}_{ij}^T \mathbf{E}_{ij} \mathbf{s} - \mathbf{s}_{(0)}^T \mathbf{E}_{ij}^T \mathbf{E}_{ij} \mathbf{s}_{(0)} \ge d_{\min}^2 \\ & (1 \le i < j \le M) \\ & \frac{1}{M}\mathbf{C}\mathbf{s} = \alpha \mathbf{c}_1 + \mathbf{c}_2 \\ & \left(\mathbf{I}_M \otimes [\mathbf{A}_{\text{tv}}]_{2,:}\right) \mathbf{s} = \frac{\mathcal{L}}{683} \cdot \mathbf{1}_M \\ & \mathbf{0} \preceq \mathbf{s} \preceq \mathbf{1} \end{array}$$

7: Set $\mathbf{s}_{(0)} = \mathbf{s}$, **go back** 6 **until** $d_{\min}$ converges.
8: **if** $d_{\min}^* < d_{\min}$

$$d_{\min}^* = d_{\min}, \ \mathbf{s}^* = \mathbf{s}$$

9: **end if**
10: **end for**
11: **end for**

IV. Numerical and Experimental Results With Commercial Quadrichromatic Clusters

In this section, using datasheets of commercial devices, we will first calculate the color-space MIMO channels formed by our proposed QLED transceiver. Then the feasible region of α, which linearizes the specified CT and CRI constraints, will be numerically evaluated. Finally, the performances of MED and bit error rate (BER) of the optimized CSK constellations are compared with the existing schemes of RGB devices under the same luminous flux and the same CT conditions.

A. Experimental Setup for Evaluation of QLEDs Color-Space MIMO Channels

Our simulations use commercially available QLED devices consisting of red, green, blue and amble colors. We chose from

[2] A software package for specifying and solving convex programs [27], [28].

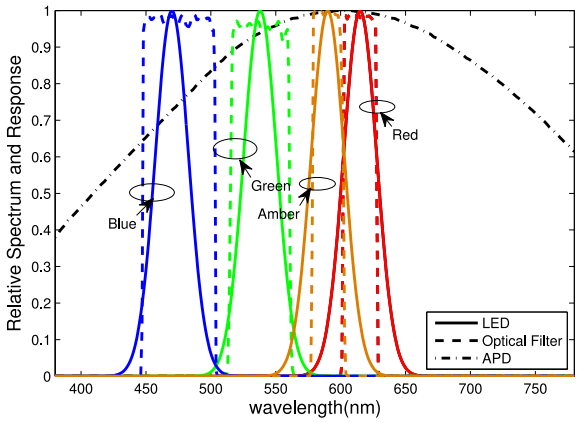

Fig. 2. Spectrum of QLED (Lumileds Luxeon C Colors), the responses of optical filters and the relative spectral response of APD in our simulation.

TABLE I
THE CMIMO CHANNELS FOR QLED-30 (RGBA(615/538/470/590) WITH 30 NM FWHM)

Rx \ Tx	FWHM=30nm			
	Red	Green	Blue	Amber
Red	0.410	0	0	0.0526
Green	0	0.353	0.0003	0.0031
Blue	0	0.0011	1	0
Amber	0.0910	0.0003	0	0.1968

the LUXEON C Color product line (LUMILEDS) [29]. The maximum luminous flux of red, green, blue and amber of a single chip are 144 lm, 204 lm, 82 lm, and 122 lm, respectively. The corresponding semi-angles at half optical power $\Phi_{1/2}$ are 162°, 170°, 170°, 162°, respectively.

We apply Si APD S5343 [30] by Hamamatsu as our PD model. The associated effective active area A is 0.78 mm^2. With a concentrator, the FOV Ψ is 60°.

To eliminate the undesirable light, we adopt Semrock Bright-Line single-band bandpass filters as our color filters. They are FF02-615/20-25 [31], FF01-538/40-25 [32], FF02-475/50-25 [33] and FF01-590/20-25 [34], respectively. The transmission curves of optical filters are plotted in Fig. 2. For better illustration, the measured relative SPD of four colors and the relative spectral response of APD are also plotted.

Assuming the angle of incident $\psi = 0^\circ$, the CMIMO channels could be evaluated by (4). The corresponding normalized channel coefficients are listed in Table I. Clearly, due to the overlaps of SPD among QLED colors, the cross-talk among color-space channels can no longer be ignored.

It should be noted that the CMIMO channels in Table I depend highly upon QLED and the optical filters. Assuming the SPD of each color LED to be Gaussian [17], we tune the full width at half maximum (FWHM) of each color from 30 nm to 40 nm, and denote them as QLED-30 and QLED-40, respectively. We can in fact use QLED-30 as RGB LEDs by disabling its amber color. Using this step, we can denote the resulting RGB LEDs from QLED-30 and QLED-40 as RGB-30 and RGB-40, respectively. We also assume that the luminous flux of each color chip are the same for fairness reason. The corresponding normalized channel coefficients [3] for QLED-40 are listed in Table II.

TABLE II
THE CMIMO CHANNELS FOR QLED-40 (RGBA(615/538/470/590) WITH 40 NM FWHM)

Rx \ Tx	FWHM=40nm			
	Red	Green	Blue	Amber
Red	0.3259	0	0	0.0701
Green	0.0004	0.3234	0.0047	0.0122
Blue	0	0.0073	0.8319	0
Amber	0.1224	0.0039	0	0.1587

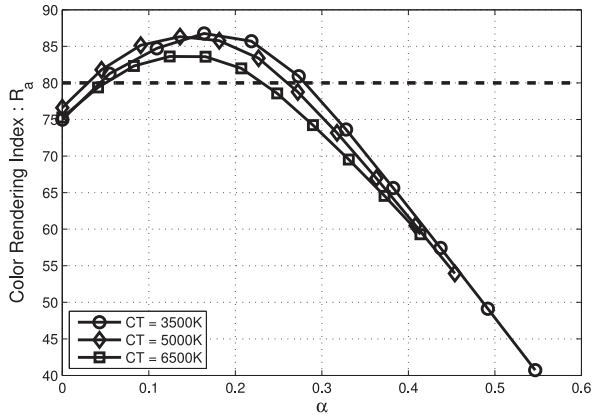

Fig. 3. The CRI curves with respect to α for warm, natural, and cool white colors with QLED-30.

We have two observations from Tables I and II:

1) The diagonal elements of QLED-30 are greater than their corresponding elements of QLED-40.
2) The crosstalk (the off-diagonal elements) of QLED-30 is less than their corresponding element of QLED-40.

These results are due to our previous fairness requirement of the same luminous flux of corresponding single color. Therefore, the SPD of QLED-40 appears flatter than that of QLED-30 and the peak value of SPD of QLED-40 is less than that of QLED-30. Consequently, with the increase of FWHM, the CMIMO channels become less and less diagonally dominant.

B. *Numerical Results of Feasible Region for α*

According to (17) in Section III-A, given a CT, the associated CRI is a function of scalar α for QLED. Owing to the entangled relationship between α and R_a, we need to numerically search the feasible region of α under the constraints of color quality, CT and CRI. The following curves in Figs. 3 and 4 illustrate how R_a would vary with α for QLED-30 and QLED-40, respectively. Clearly, the α feasible region that $R_a \geq \beta$ can be numerically obtained. Typically, the minimum CRI requirement β is at least 80 [35].

Three concave-shape curves are shown in Figs. 3 and 4 for three color temperature types, 3500 K (warm), 5000 K (natural), 6500 K (cool) white, respectively. We have three observations:

[3]To compare the CMIMO channels of QLED-30 with that of QLED-40, we apply normalization with respect to the maximum value of two CMIMO channels.

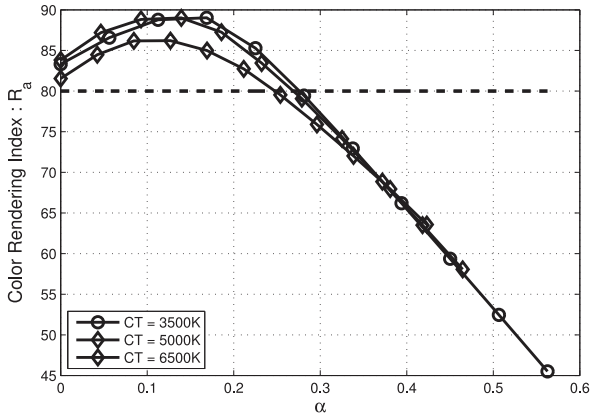

Fig. 4. The CRI curves with respect to α for warm, natural, and cool white colors with QLED-40.

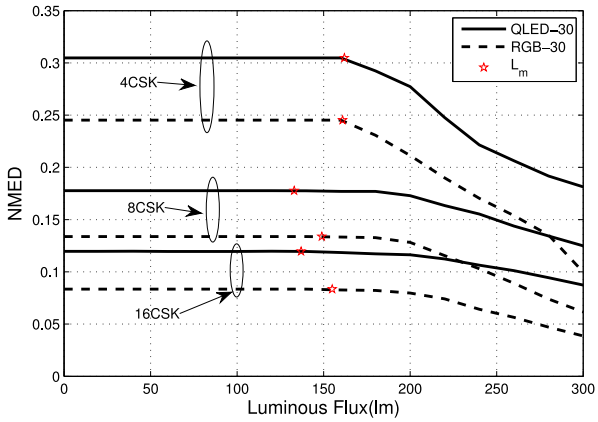

Fig. 5. The luminous flux normalized MED performances of QLED-30 and RGB-30 LED under CT 5000 K by varying luminous flux.

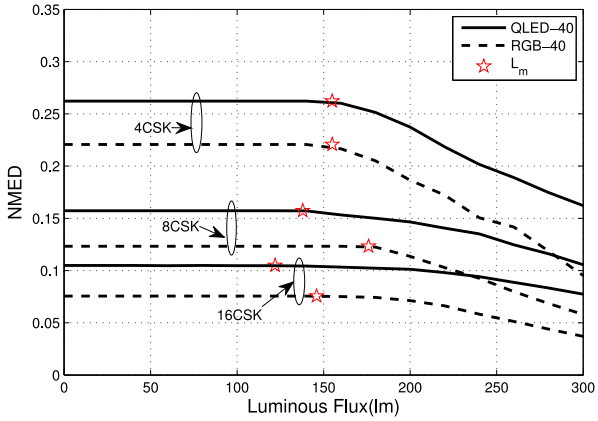

Fig. 6. The luminous flux normalized MED performances of QLED-40 and RGB-40 LED under CT 5000 K by varying luminous flux.

1) According to (9), α is in fact the volume of amber color. Consequently, R_a associated with $\alpha = 0$ is precisely the one achieved with RGB LEDs. Clearly, with the help of additional amber color, the achieved CRIs could be further improved for any of the three color types: warm, natural, and cool white. Hence, the additional color in QLED is critical for CRI improvement of polychromatic clusters.
2) When the number of wavelengths exceeds three, as long as the minimum CRI requirement β is reasonable, we generally have a set of operating points instead of only one point to map to a specified color temperature (CT). Suppose the required CRI is higher than 80, which is a common for workplace illumination and could be found generally in the data sheet of commercial LED [35]. The corresponding region of feasible α can be numerically determined as follows. For QLED-30: in the case of 3500 K, the feasible range of alpha is $0.0423 \leq \alpha \leq 0.280$; in the case of 5000 K, $0.0296 \leq \alpha \leq 0.2600$; whereas, for the case of 6500 K, $0.0501 \leq \alpha \leq 0.2310$. For QLED-40: in the case of 3500 K, the feasible range of alpha is $0 \leq \alpha \leq 0.2670$; in the case of 5000 K, $0 \leq \alpha \leq 0.2689$; whereas, in the case of 6500 K, $0 \leq \alpha \leq 0.2477$. Unless otherwise specified, we shall apply these alpha regions in the following simulations.
3) According to Figs. 3 and 4, with the increase of FWHM, the achieved CRI is generally improved, and the feasible region of amble light also becomes larger. Since broader SPD of each primary color improves the continuity of the synthesized SPD which generally benefits the CRI.

C. The Minimum Euclidean Distance

In this part, we will investigate the MED performance of the optimized received constellations. Note that, the MED generally is a rather complex function of luminous flux $\mathcal{L}$. To reveal the intrinsic of CSK constellation design, we will plot the luminous flux normalized minimum pairwise Euclidian distance (NMED) instead of MED directly:

$$d_{\text{NMED}} \triangleq \frac{1}{\mathcal{L}} \cdot d_{\text{MED}}$$

Fig. 5 demonstrates the NMED performance under CT 5000 K for QLED-30 and RGB-30 LEDs, respectively, for various levels of luminous flux.

It can be seen from the NMED curves that the MED does not always proportionally increase with luminous flux $\mathcal{L}$. Specifically, the MED would linearly increase with $\mathcal{L}$ until $\mathcal{L}$ moves beyond some threshold $\mathcal{L}_m$ (denoted with red asterisks in Fig. 5), e.g., with a 16-CSK, $\mathcal{L}_m = 137$ lm for QLED-30, or $\mathcal{L}_m = 155$ lm for RGB-30 LED. This phenomenon will be better explained in next section using the visualization of constellation evolution with luminous flux. Note that, the optimized constellation for QLED-30 always achieves larger MED than that of RGB-30 LED. At the same time, larger constellation size would however lead to lower MED value. Similar results can be observed in Fig. 6 for QLED-40 and RGB-40, respectively.

To illustrate the effect of FWHM of LED SPD and the associated CMIMO channels, we should compare Figs. 5 with 6. Clearly, QLED-30 with 4, 8, and 16 CSK obtain larger NMED than QLED-40 with 4, 8, and 16 CSK, respectively, because of the more diagonally dominant CMIMO channels shown in Tables I and II. Combined with the CRI results from the previous section, we find that broader FWHM achieves higher CRI but worse NMED, whereas narrower FWHM achieves lower CRI but better NMED. These results and observations demonstrate a

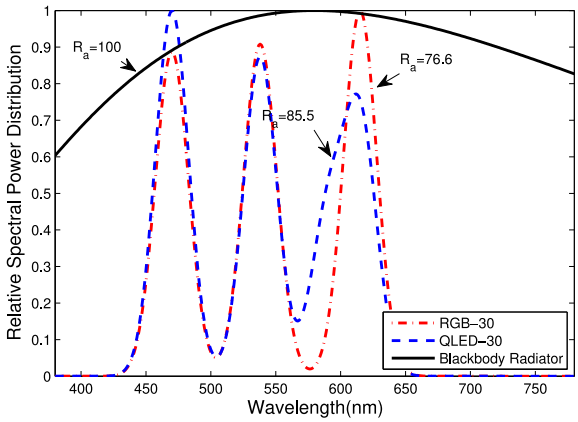

Fig. 7. The relative SPDs of the white light generated by 16 CSK constellation designed with CT 5000 K and 300 lm for QLED-30 and RGB-30, respectively. The SPD of blackbody radiator is with 5000 K.

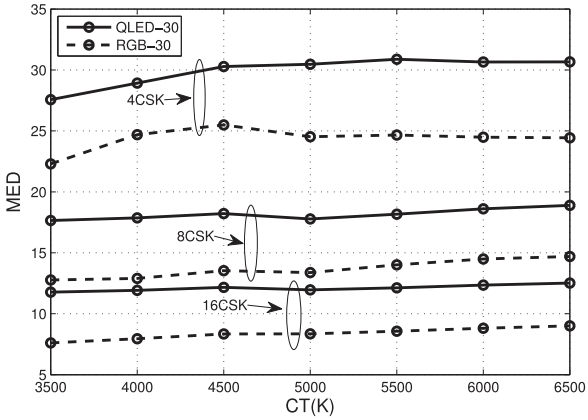

Fig. 8. The MED performances of QLED-30 and RGB-30 LEDs by varying CT with 60 lm.

general tradeoff between illumination and communication with respect to the FWHM of LED SPD.

To better illustrate the improvement of color qualities of QLED-30, the relative spectral power distribution of white light, generated for 16 CSK constellation under 60 lm and CT 5000 K, and the associated CRI value R_a for QLED-30 and RGB-30 are shown in Fig. 7, respectively. Clearly, QLED-30 obtains better CRI than RGB-30.

Next, we examine the MED performance by varying color temperature and constellation size at 60 lm in Figs. 8 and 9 for multi-color LED with 30 nm FWHM and multi-color LED with 40 nm FWHM, respectively. For all the tested constellation sizes in our simulation, the MEDs of QLED (QLED-30 and QLED-40) constellations outperform those of RGB (RGB-30 and RGB-40) constellations for CT from 3500 K to 6500 K. For high constellation size, simulation results show that the MED tends to remain steady from warm to cold color temperature. Thus, for a given luminous flux, CT adjustment does not noticeably impact the link performance. Also note that for all color temperatures from 3500 K to 6500 K, the MED performances of QLED-30 are always better than those of QLED-40. Since both cases fulfill the minimum CRI requirement, it makes sense for us to focus on QLED-30 henceforth in the following experiments.

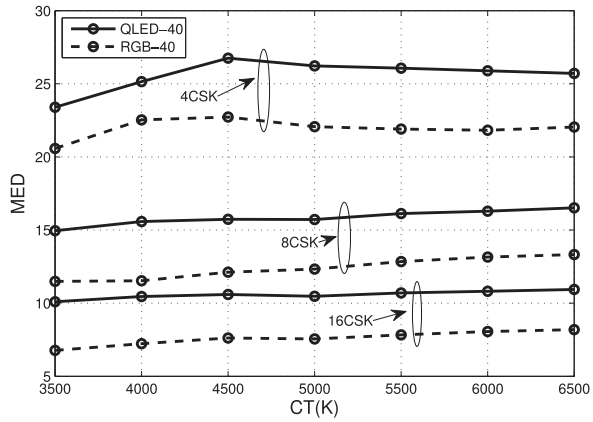

Fig. 9. The MED performances of QLED-40 and RGB-40 LEDs by varying CT with 60lm.

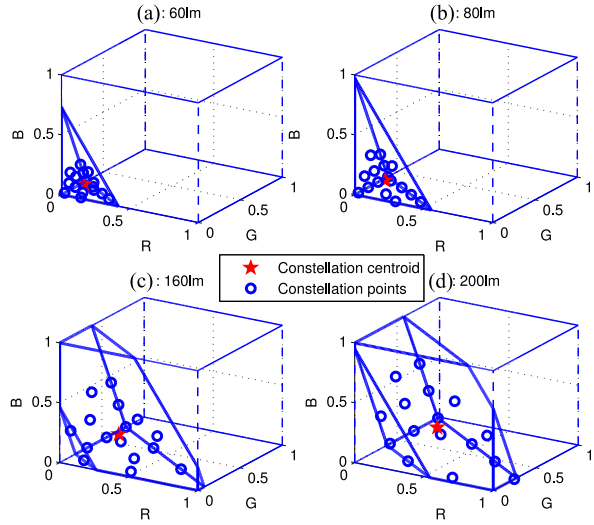

Fig. 10. Evolution of 16 CSK constellations of QLED-30 with the increase of luminous flux under 5000 K CT and $R_a \geq 80$.

D. Luminous Flux Independent CSK Constellation Design

To better understand the NMED curve bend phenomenon in Figs. 5 and 6, the constellations of QLED should be illustrated by ignoring the coordinate of amble light, which projects 4-D constellations into 3-D constellations.

In Fig. 10(a)–(d), blue points are the optimized 16 CSK constellations of QLED-30 at CT 5000 K. The red starts represent the constellation centroid, which satisfy all illumination requirements such as CT, CRI and luminous flux. In each sub-figure, an internal space $\mathcal{S}$ enclosed by bold lines represents the joint space confined by the luminous flux constraint (8d) and constellation amplitude constraints (8f), and the tilted planes on the boundary of $\mathcal{S}$ are obtained by setting the coordinate of amble light '0' and '1' in (8d), respectively. Note that, in Fig. 10(a)–(b), there is only one tilted plane since the other one does not intersect with the space confined by (8f).

When the luminous flux is sufficiently small ($\mathcal{L} = 60$ lm in Fig. 10(a)), the optimized constellations tend to cluster closer and many of the constellation points would lie in the internal of $\mathcal{S}$. With increasing luminous flux, the optimized constellations

in fact would linearly expand as shown in Fig. 10(b). Obviously, the linear expansion of constellations will enlarge MED linearly without modifying color qualities CT and CRI. When the luminous flux reaches $\mathcal{L}_m$, there is no more room for constellations to linearly expand. Consequently, constellation distribution would now have to change in order to accommodate higher luminous flux requirement. This effect is shown in Fig. 10(c)–(d) as most of constellation points would consequently lie on the boundary of $\mathcal{S}$. Therefore, the MED increase from further increase of luminous flux would inevitably decrease as a result.

Finally, as long as the luminous flux of a multi-color LED stays below $\mathcal{L}_m$, a flux independent constellation can always be designed by optimizing the constellation points $\bar{\mathbf{s}}_i$, $i = 1, \cdots, M$, defined in (5), at some low luminous flux. In this case, $\gamma_{\max}$, the maximum allowed value of dimming control factor γ, is therefore obtained by

$$\gamma_{\max} = \frac{1}{\max\limits_{i,j} \bar{\mathbf{s}}_{i,j}}$$

whose value equals $\mathcal{L}_m$ as long as $\bar{\mathbf{s}}_i$ is optimized at $\mathcal{L} = 1$ lm. In addition, the red stars in Figs. 5 and 6 are our predicted $\mathcal{L}_m$. Figs. 5 and 6 indicates that our predictions closely match our simulation results. When the demand of luminous flux exceeds $\mathcal{L}_m$, more multi-color LEDs should be employed and be turned on to guarantee that the luminous flux of each multi-color LED is less than $\mathcal{L}_m$, which also in turn contributes to each multi-color LED chip life expectancy.

E. Bit Error Rate Performance

In this section, to better demonstrate the effect of MED maximization, we numerically evaluate the bit error rate performance. Specifically, each frame of 4000 bits are encoded by an LDPC code of rate $R = 2/3$ for error correction. The code is constructed with the protograph [36] of the code in 802.16e [37] by applying the improved progressive-edge-growth (PEG) algorithm [38]. The LDPC-coded bits are then mapped to CSK constellation points based on the binary switching algorithm (BSA) [39] to minimize the BER.

To be consistent with our experimental validation, in the simulation, the symbol rate is set to 12 MHz. Therefore, the information rate of 4, 8 and 16 CSK are 12, 24 and 32 Mbps, respectively.

Next we define the energy per bit to noise ratio as

$$\frac{E_b}{N_0} \triangleq \frac{1}{\log_2 M} \cdot \frac{||(\mathbf{I}_M \otimes \mathbf{H})\,\mathbf{s}||^2}{M\sigma_n^2}$$

where σ_n^2 is the noise variance that accounts for the averaged shot noise and circuit thermal noise [10]. This metric is common in BER performance evaluation for multi-channel systems and was also employed in [10] for QLED VLC performance evaluations.

For receivers to optimize BER performance, we adopt the *maximum a posteriori* (MAP) symbol detector to generate the soft input (likelihood-ratio) for the LDPC decoder. A standard sum-product algorithm (SPA) is employed, and the maximum iteration number of decoding is limited to 100.

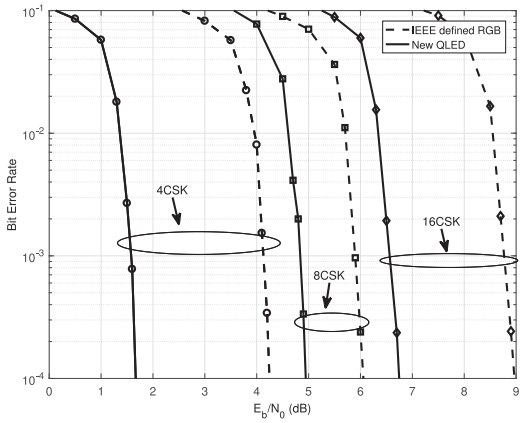

Fig. 11. BER performances of QLED and RGB LEDs achieving the same apparent light of IEEE 802.15.7 CBC-2.

For simplicity, our proposed constellation design with QLED-30 is labeled as 'QLED'. And four existing constellation designs with multi-color LEDs are also considered as benchmarks for performance comparison:

1) The CSK constellation proposed by IEEE 802.15.7 [40] is denoted with 'IEEE defined RGB'.
2) The CSK constellation design proposed in [14] is denoted with 'RGB'.
3) The simple single carrier WDM scheme for QLED device is labelled as 'QLED SC WDM'. Specifically in this scheme, each color channel (wavelength) uses a standard PAM modulation. To generate a proper CT and CRI, the averaged intensity of each color should exactly match to the averaged intensity of its counterpart. At the same time, we scale the constellation of the 'QLED SC WDM' scheme to maximize its BER performance without violating the amplitude constraint.
4) The CSK constellation design proposed in [10] for QLED is labelled as 'QLED-[10]'.

1) BER Comparison with IEEE defined CSK Constellation: Since the color space spanned by the IEEE defined RGB LEDs used in standard [41] is much wider than that spanned by our chosen QLED, to fairly compare with the performance of IEEE CSK constellations, we define a new QLED by adding 590 nm monochromatic amber light to IEEE defined RGB LEDs. This new QLED device will only be used in comparison with IEEE CSK standard. We synthesize the same apparent light using the new QLED (*with the same tri-stimulus values*) of IEEE CSK, and we further remove the CRI constraint (13). The performance results are illustrated in Fig. 11 for 4, 8, 16 CSK constellations of colour band combination (CBC) 2 defined in [41].

Our proposed QLED constellation designs outperform IEEE constellation by more than 1 dB gain at 10^{-3} BER. From our analysis, the performance gain has two contributing factors: First, the IEEE constellations are directly designed on the chromaticity diagram while our proposed QLED constellation design is optimized in the received signal space; Second, with the help of the extra amble light channel the BER performance provides larger diversity gain.

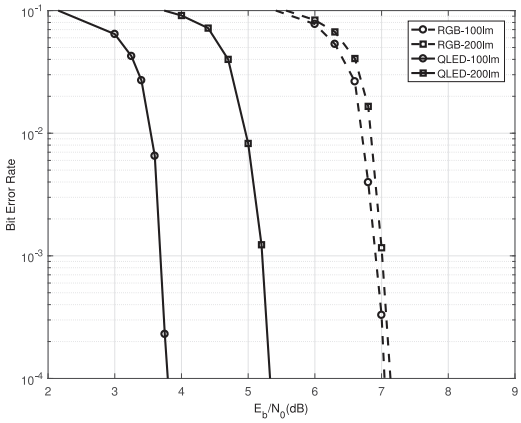

Fig. 12. BER performance comparison for 4 CSK between QLED and RGB LEDs at 100 lm and 200 lm, respectively.

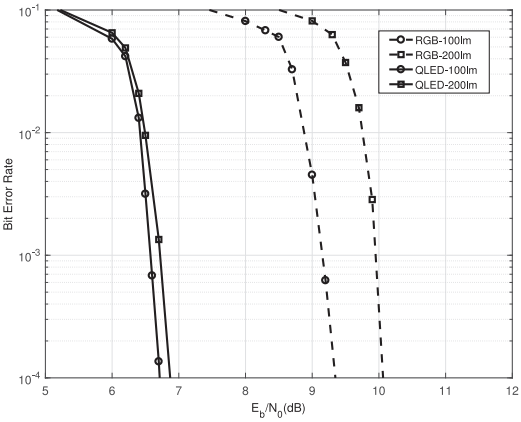

Fig. 13. BER performance comparison for 8 CSK between QLED and RGB LEDs at 100 lm and 200 lm, respectively.

2) BER Comparison With Constellation Design Proposed in [14] for RGB LED: To further demonstrate the important impact of the extra amble light channel, BER performances of QLED with 4 CSK constellations are then compared with the counterpart of RGB LEDs, in Fig. 12. The CSK constellations are designed at $\mathcal{L} = 100$ lm $\leq \min\{\mathcal{L}_{m,\text{RGB}}, \mathcal{L}_{m,\text{QLED}}\}$, $\mathcal{L} = 200$ lm $\geq \max\{\mathcal{L}_{m,\text{RGB}}, \mathcal{L}_{m,\text{QLED}}\}$ for QLED and RGB LEDs, respectively.

From Fig. 12, we observe that the BER performance of the optimized QLED constellation is clearly superior to that optimized for RGB LEDs, providing a 3 dB SNR gain at 100 lm 10^{-3} BER due to 0.06 NMED gap shown in NMED Fig. 5. Furthermore, still at 10^{-3} BER, the constellation design for QLED under 100 lm is also 1.5 dB better than that design for QLED under 200 lm, which matches the NMED gap shown in Fig. 5. Consequently, our proposed luminous flux independent CSK constellation can be employed and the luminance of each multi-color LED would not exceed $\mathcal{L}_m$. Similar performances are also observed in Figs. 13 and 14 for 8 CSK and 16 CSK, respectively. It should be noted that, in light of the small NMED gap between the constellation designed for both QLED and RGB LEDs, respectively, under 100 lm and those under 200 lm, the corresponding BER performance gap is also narrow.

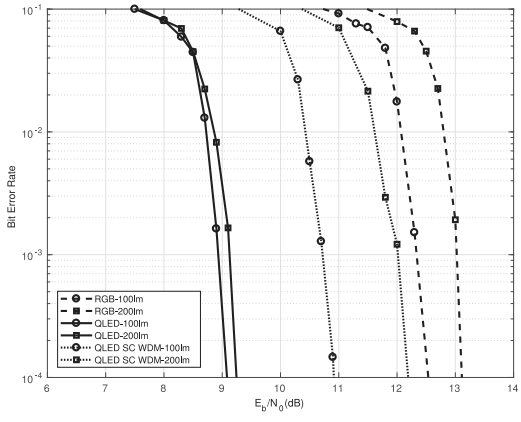

Fig. 14. BER performance comparison for 16 CSK, 'QLED SC WDM' scheme and RGB LEDs at 100 lm and 200 lm, respectively.

In Fig. 14, the 'QLED SC WDM' scheme for QLED is also tested for comparison. Every color channel sends the 2-level PAM signal. It should be noted that despite the fact that the 'QLED SC WDM' scheme shares the same CT and CRI properties of illumination with our proposed 16 CSK scheme, our proposed CSK constellation maintains a steady illumination across the constellation, whereas the 'QLED SC WDM' scheme would suffer potentially from the intensity-flicking problem. Furthermore, our proposed 16 CSK modulation outperforms the 'QLED SC WDM' scheme by more than 1.5 dB for two different illumination cases.

Our proposed CSK modulation benefits from two important facts:

1) CSK constellation could be viewed as a joint constellation design for 'QLED SC WDM' scheme. In our proposed algorithm, the target minimum pairwise Euclidean distance is always maximized (MED=11.94@100 lm and MED=23.24@200 lm), whereas the MED of 'QLED SC WDM' scheme is not optimized (MED=10.07@100 lm and MED=5@200 lm).
2) Our CSK symbol detector is a joint detector for CMIMO channel with MAP criterion, while the 'QLED SC WDM' scheme does not utilize the diversity provided by CMIMO channel as it treats crosstalk merely as noises.

3) BER Comparison With CSK Constellation for QLED Proposed in [10]: In this part, we will compare our proposed CSK design with the CSK constellation for QLED recently reported in [10]. Since our QLED spectra are quite different from those used in [10], we decide to adopt the same QLED proposed in Fig. 5 of [10] for a fair comparison. Furthermore, our proposed constellation centroid will be set to the same as the one in [10], whose the chromaticity values are $(0.329, 0.332)$, which is close to day-light setting with CT $= 6500$ K. For the same reason as stated in Section IV-E1, we are unable to evaluate the CRI value for these QLEDs due to the lack of published spectrum information. Consequently, we did not enforce the CRI constraint (8e). We also adopt the CMIMO channel given by [10, eq. (13)] to design our CSK constellation.

The BER performances are shown in Fig. 15. Clearly, our proposed CSK constellation is able to achieve better BER

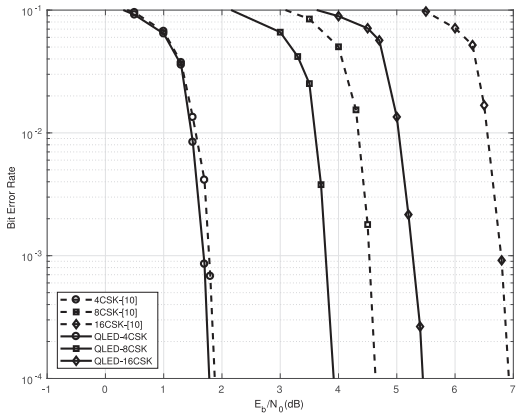

Fig. 15. BER performance comparisons for 4,8 and 16 CSK, respectively, proposed in [10] and our proposed algorithm.

TABLE III
THE NMED COMPARISON BETWEEN CSK CONSTELLATION OF THOSE PROPOSED IN [10] AND OUR PROPOSED METHOD

Constellation	[10]	Ours
4 CSK	0.2901	0.2902
8 CSK	0.1451	0.1512
16 CSK	0.0967	0.1079

performance than that from the proposed design of [10]. Moreover, as the constellation size increases, the BER performance gap grows quickly, from 0.1 dB to 1.1 dB at 10^{-3} BER. From our analysis, the performance gain can be attributed to two sources: (1) The constellation design in [10] is directly operated on the chromaticity diagram, whereas ours are designed on received signal space. In Table III, NMEDs of both constellations are listed, respectively. We observe similar NMED gaps for both constellations. Thus, NMED is an important metric to optimize system performance. (2) Our design fully considers the channel effect. In other words, if the crosstalk in the CMIMO channel is stronger, the performance gap could grow larger.

F. Complexity Discussions

In this section, we will examine the complexity issues involved in CSK modulation. Generally speaking, the complexity in CSK modulation consists of two parts: complexity in constellation design and the complexity in symbol demodulation.

First, the 'QLED SC WDM' scheme is the least complex in CSK design and symbol detection, since its constellation design is independent for each color channel. Furthermore, the symbol detection for each color channel is also independent. On the other hand, the performance is the worst among comparison schemes.

Another low complex scheme is the class of the CSK constellation proposed in [10] and [41]. Since the constellation design operates on the chromaticity diagram, the solution is independent from the CMIMO channel experienced by signals. Consequently, as shown in Figs. 11–14, the BER performance is inferior to that of our proposed CSK design. On the other hand, its symbol detection has the same complexity as that for our proposed CSK modulation when utilizing MAP detection and the joint detection-decoding principle.

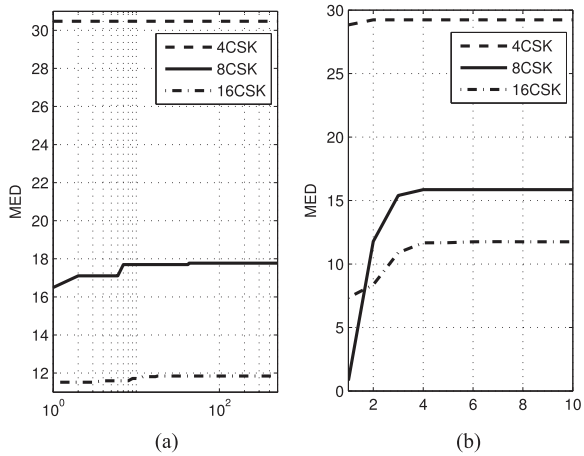

Fig. 16. The convergence speed of the second and the third loop, respectively, in our proposed iterative CSK constellation design. (a) Number of random trial. (b) Iteration number of the third loop.

Finally, similar to the CSK constellation design in [14], our proposed CSK constellation design is more complex. Unlike the CSK designs proposed in [10] and [41], we propose to maximize the MED of CSK constellation in the received signal space. Consequently, the CMIMO channel should be known or estimated before constellation design. Fortunately, unlike in RF systems, CMIMO channel of VLC is reasonably stable such that frequent channel state information (CSI) feedbacks would be unnecessary. As discussed in Section II-B, usually the line-of-sight (LOS) channels could well support high speed VLC system. Furthermore, the VLC CMIMO channel is mainly affected by the spectrum overlaps of LEDs and color filters. Therefore, we are able to design the entire set of our CSK constellations a priori once the model of QLED and color filter have been chosen, before activating one of the pre-designed constellations in realtime communications based on the channel conditions.

Next, we would like to provide some numerical results on the complexity of proposed constellation design algorithm. There are three nested loops in our proposed constellation design.

The first loop from steps 2 to 11 sequentially scans CRI feasible regions. Since the original CSK design problem in (9)–(14) is non-convex, our proposed search in the third loop from steps 5 to 7 would only generate a sub-optimum result. Therefore, randomly enumerating the initial point of the convex optimization (the 4th step) in the second loop is necessary and helpful. Usually, a large number of random trials can help identify a good solution. Fig. 16(a) demonstrates the variation of the maximal MED with respect to random initialization trials.

Clearly, after 50 random trials, the result of the maximum MED search is quite steady. Thus in practice, we suggest that 50 trials would be desired.

The third loop is for the linear low-bound approximation in (12). The convex optimization should be implemented enough times to allow MED to approach the maximal value. In Fig. 16(b), the effect of the iteration number for the third loop is illustrated. Usually, 5–10 iterations are enough to achieve

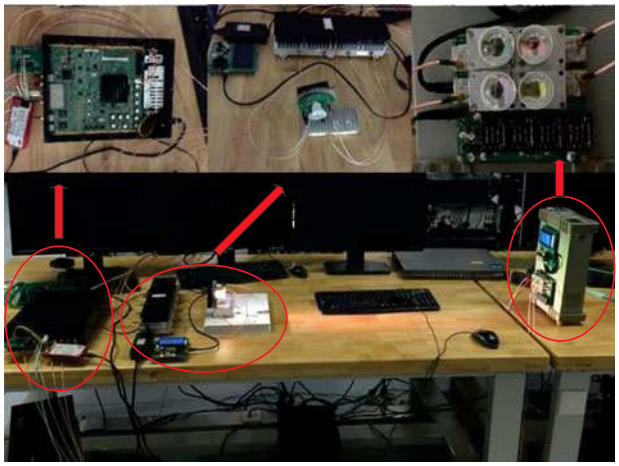

Fig. 17. Experimental testbed for visible light communications with QLED.

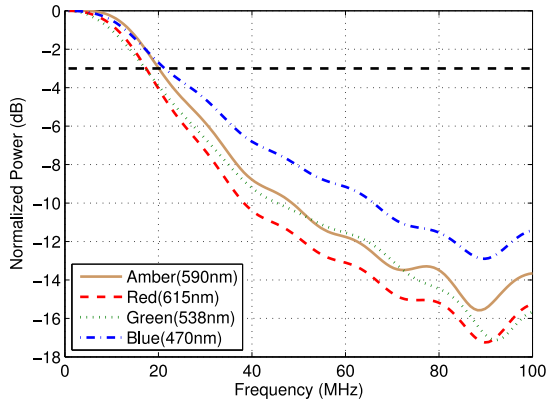

Fig. 18. Measured frequency responses of our VLC testbed with QLED (product of LUMILEDS).

convergence to near optimality. In addition, the worst-case complexity of step 6 (a second-order cone programming (SOCP) [26]) in our proposed iterative CSK constellation optimization is

$$O\left(\left(1+\frac{1}{2}M(M-1)\right)^{\frac{1}{2}}(2M(M-1)+25)\right)$$

where M is the constellation size of CSK modulation.

G. Experimental Results and Discussions

To better verify the performance of our proposed CSK constellation, we will experimentally measure the BER performance with our multi-color VLC testbed.

As shown in Fig. 17, we used the Xilinx FPGA platform to carry out signal processing. The LDPC encoder and the method of coded bit mapping are identical to those adopted in numerical simulations described in Section IV-A. Furthermore, key devices such as QLED, color filters and APD, are also identical to those used in our numerical simulations. The distance between the transmitter and receiver is set to 80 cm.

First, the measured frequency responses for red/green/blue/amble color LEDs are shown in Fig. 18. Clearly, to fully eliminate the impact of inter-symbol interference, we limit the symbol rate up to 12 MHz, which is much less than the minimum 3 dB bandwidth (18 MHz) of four colors. It should be noted that our measured bandwidth is without pre-equalization.

TABLE IV
THE MEASURED CMIMO CHANNELS FOR QLED (615NM/538NM/470NM/590NM)

Rx \ Tx	Red	Green	Blue	Amber
Red	0.3627	0.0010	0.0017	0.0082
Green	0.0005	0.4249	0.0100	0.0018
Blue	0.0033	0.0295	1.0000	0.0021
Amber	0.0244	0.0141	0.0372	0.3093

TABLE V
THE 4 CSK CONSTELLATION FOR QLED AND RGB IN EXPERIMENTAL TEST

RGB LEDs			QLED			
R	G	B	R	G	B	A
0.6195	0.0529	0	0.4411	0.1788	0	0
0	0.3837	0.2648	0	0.4902	0	0
0.2963	0.253	0.0699	0	0.0564	0	0.7253
0	0.4902	0	0	0.2262	0.3364	0.2154

TABLE VI
THE 8 CSK CONSTELLATION FOR QLED AND RGB IN EXPERIMENTAL TEST

RGB LEDs			QLED			
R	G	B	R	G	B	A
0.4301	0.1347	0.1291	0.2358	0.0890	0	0.3925
0.2457	0.2642	0.1308	0	0.1371	0.1915	0.4617
0.5488	0.1028	0	0	0	0	0.8197
0.1806	0.3627	0	0	0.3943	0.2385	0
0	0.4902	0	0.2386	0.4902	0	0
0	0.3782	0.2787	0	0.2049	0.2429	0.0321
0.3613	0.2352	0	0.3311	0.2943	0	0.3276
0.0651	0.3917	0.1308	0	0.2565	0	0

At the receiver, the data from 4 wavelength channels are sampled and stored by our testbed for off-line processing and error performance evaluations. The overall CMIMO channel is estimated and described in Table IV. Clearly, our measured CMIMO channel is not same as those in our Table IV which was used in our numerical stimulations. Such differences might be caused by the parameter mismatch of color-mixing lens and receiving lens, the misalignment of the angle of incident, or the crosstalk in electrical signals, among others. Nevertheless, once the CMIMO channel is measured, the CSK constellation could be designed off-line and is stored in both transmitter and receiver for communication.

CSK constellations of sizes 4, 8 and 16 for QLED and TLED are listed in Tables V–VII, respectively. All of them are designed with the same constraints: CT $= 5000$ K and $\mathcal{L} = 100$ lm. For QLED, the additional constraint CRI ≥ 80 is also included. Accordingly, the information data rate are 16 Mbps, 24 Mbps and 32 Mbps, respectively.

In Fig. 19, we demonstrate the measured BER performances for the constellation given in Tables V–VII, respectively. The E_b/N_0 is precisely tuned by digitally adjusting the signal output amplitude from D/A.

Similar to our numerical simulations described in the previous section, our experimental results verified that the CSK constellation for QLED outperforms those designed for TLED.

TABLE VII
THE 16 CSK CONSTELLATION FOR QLED AND RGB IN EXPERIMENTAL TEST

RGB LEDs			QLED			
R	G	B	R	G	B	A
0.3754	0.193	0.0801	0.3823	0.1102	0	0.1842
0	0.4222	0.1693	0.1718	0.3689	0	0
0.1144	0.4095	0	0	0.2146	0.1263	0.3760
0.6673	0.0192	0	0	0.1503	0	0.5684
0.3355	0.2533	0	0	0.4902	0	0
0.4461	0.1753	0	0	0.3212	0	0.2826
0.1105	0.3439	0.1698	0.2150	0.1516	0.1593	0.2053
0	0.4902	0	0	0.3619	0.3192	0
0.1542	0.3491	0.0801	0.1704	0.1992	0	0.2853
0.2648	0.2711	0.0801	0.3437	0.2476	0	0
0.5567	0.0972	0	0	0.0192	0	0.7876
0.225	0.3314	0	0	0.2414	0.2789	0.2285
0	0.3855	0.2606	0.1237	0.2923	0.1455	0.0871
0.2211	0.2659	0.1698	0.2119	0.0612	0	0.4672
0.0419	0.4288	0.0791	0	0.4260	0.1596	0
0.1503	0.2836	0.2499	0	0.0806	0.1572	0.5793

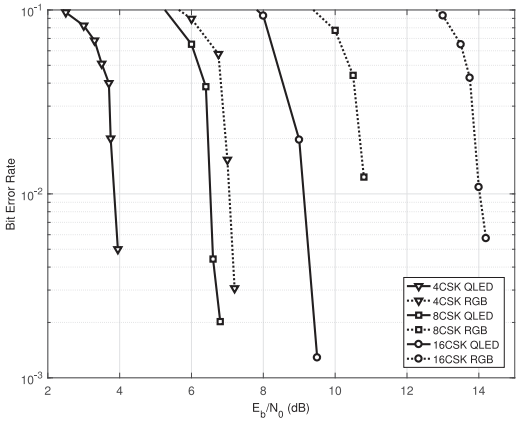

Fig. 19. Measured BER performance for QLED and RGB LEDs, respectively.

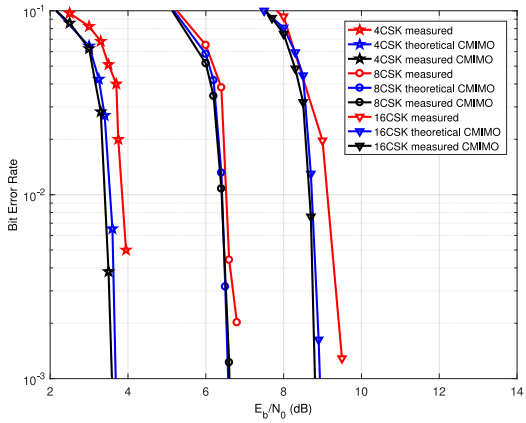

Fig. 20. BER performance comparison between measurement result and simulation result.

Furthermore, the BER performance gap grows with an increasing constellation size.

In Fig. 20, our experimentally measured BER performance, labelled as 'measured', is also compared with two simulated BER performances for QLED device. Specifically, the first simulated BER performance, labelled as 'theoretical CMIMO', is for the theoretical CMIMO channel (in Table I), which has already been shown in Figs. 12–14, respectively, for 4 CSK, 8 CSK and 16 CSK constellation. The second simulated BER performance, labelled as 'measured CMIMO', is for the measured CMIMO channel (in Table IV) with the associated constellation in Tables V–VII, respectively.

Clearly, the gap between our measured BER performance and the simulated BER performances are no more than 0.5 dB. Although our measured CMIMO channel is not same as the theoretical CMIMO channel, the simulated BER performances with measured CMIMO channel are slightly better than those results with our theoretical CMIMO. Since the diagonal elements of our measured CMIMO channel are larger than the corresponding elements in the theoretical CMIMO channel. Finally, based on our measurements, we conclude that our experimental tests could validate the performance of our proposed CSK constellation design.

It should be noted that our current CSK data rate is relative low, e.g., no more than 32 Mbps. The data rate of our experimental VLC testbed could be further improved through following schemes:

1) *Bandwidth Extension:* Our LED bandwidth is 18 MHz. To extend the bandwidth, we could employ the pre-equalization method proposed in [42]. The reported bandwidth is extended to 66 MHz.
2) *Larger Constellation Size:* In our simulations, the constellation size is at most 16. We could improve our data rate by utilizing 64 CSK or larger constellation size.
3) *Increasing Signal Noise Ratio:* Although we could enhance the data rate by increasing constellation size, the BER performance is also limited by the SNR of received signal. Higher SNR can lead to higher data rate by levering stronger transmit power amplifiers.
4) *Better Receivers:* More sophisticated receivers allow the transmitter to utilize much wider bandwidth (e.g., 10 dB bandwidth). The cost is the complexity of the receiver algorithm.

V. CONCLUSION

This work investigates a CSK constellation design for the new quadrichromatic LED chips by jointly considering various illumination qualities, such as color temperature, color rendering index and luminous flux in practical VLC applications. Our proposed algorithm tackles the original design problem by numerically linearizing the CT and high complicated CRI constraints. We maximize the minimum pairwise Euclidean distance to iteratively obtain good CSK constellation designs for commercial grade multi-color LED chips. Our MED performance results indicate the existence of a luminous flux independent constellation design for QLED. Under the same luminous flux and CT constraints, our proposed CSK constellation substantially improves the resulting MED and BER performances over RGB based CSK systems. Moreover, our solution can deliver truly high luminous color quality and can also prolong LED life expectancy.

REFERENCES

[1] E. Schubert and J. Kim, "Solid-state light sources getting smart," *Science*, vol. 308, no. 5726, pp. 1274–1278, May 2005.

[2] J. Vučić, C. Kottke, S. Nerreter, K.-D. Langer, and J. Walewski, "513 Mbit/s visible light communications link based on DMT-modulation of a white LED," *J. Lightw. Technol.*, vol. 28, no. 24, pp. 3512–3518, Dec. 2010.

[3] C. Gong, S. Li, Q. Gao, and Z. Xu, "Power and rate optimization for visible light communication system with lighting constraints," *IEEE Trans. Signal Process.*, vol. 63, no. 16, pp. 4245–4256, Aug. 2015.

[4] Y. Wang, X. Huang, L. Tao, J. Shi, and N. Chi, "4.5-Gb/s RGB-LED based WDM visible light communication system employing CAP modulation and RLS based adaptive equalization," *Opt. Express*, vol. 23, no. 10, pp. 13 626–13 633, May 2015.

[5] Y. Wang, L. Tao, X. Huang, J. Shi, and N. Chi, "8-Gb/s RGBY LED-Based WDM VLC system employing high-order CAP modulation and hybrid post equalizer," *IEEE Photon. J.*, vol. 7, no. 6, pp. 1–7, Dec. 2015.

[6] A. Khalid, G. Cossu, R. Corsini, P. Choudhury, and E. Ciaramella, "1-Gb/s transmission over a phosphorescent white LED by using rate-adaptive discrete multitone modulation," *IEEE Photon. J.*, vol. 4, no. 5, pp. 1465–1473, Oct. 2012.

[7] S. Rajagopal, R. D. Roberts, and S.-K. Lim, "IEEE 802.15.7 visible light communication: Modulation schemes and dimming support," *IEEE Commun. Mag.*, vol. 50, no. 3, pp. 72–82, Mar. 2012.

[8] H. Elgala, R. Mesleh, and H. Haas, "An LED model for intensity-modulated optical communication systems," *IEEE Photon. Technol. Lett.*, vol. 22, no. 11, pp. 835–837, Jun. 2010.

[9] J. Armstrong and B. J. C. Schmidt, "Comparison of asymmetrically clipped optical OFDM and DC-biased optical OFDM in AWGN," *IEEE Commun. Lett.*, vol. 12, no. 5, pp. 343–345, May 2008.

[10] R. Singh, T. OFarrell, and J. P. David, "An enhanced color shift keying modulation scheme for high-speed wireless visible light communications," *J. Lightw. Technol.*, vol. 32, no. 14, pp. 2582–2592, Jul. 2014.

[11] R. J. Drost and B. M. Sadler, "Constellation design for color-shift keying using billiards algorithms," in *Proc. Globecom Workshops*, Dec. 2010, pp. 980–984.

[12] E. Monteiro and S. Hranilovic, "Constellation design for color-shift keying using interior point methods," in *Proc. Globecom Workshops*, Dec. 2012, pp. 1224–1228.

[13] E. Monteiro and S. Hranilovic, "Design and implementation of color-shift keying for visible light communications," *J. Lightw. Technol.*, vol. 32, no. 10, pp. 2053–2060, May 2014.

[14] Q. Gao, R. Wang, Z. Xu, and Y. Hua, "DC-informative joint color-frequency modulation for visible light communications," *J. Lightw. Technol.*, vol. 33, no. 11, pp. 2181–2188, Jun. 2015.

[15] S. Pergoloni, M. Biagi, S. Rinauro, S. Colonnese, R. Cusani, and G. Scarano, "Merging color shift keying and complementary pulse position modulation for visible light illumination and communication," *J. Lightw. Technol.*, vol. 33, no. 1, pp. 192–200, Jan. 2015.

[16] Y. Ohno, "Color rendering and luminous efficacy of white LED spectra," in *Proc. SPIE*, Oct. 2004, vol. 5530, pp. 88–98.

[17] M. S. Shur and R. Zukauskas, "Solid-state lighting: Toward superior illumination," in *Proc. IEEE*, vol. 93, no. 10, pp. 1691–1703, Oct. 2005.

[18] A. Zukauskas, F. Ivanauskas, R. Vaicekauskas, M. S. Shur, and R. Gaska, "Optimization of multichip white solid state lighting source with four or more LEDs," in *Proc. SPIE*, 2001, vol. 4445, pp. 148–155.

[19] A. Zukauskas *et al.*, "Quadrichromatic white solid state lamp with digital feedback," in *Proc. SPIE*, 2004, vol. 5187, pp. 185–198.

[20] G. Cossu, A. Wajahat, R. Corsini, and E. Ciaramella, "5.6 Gbit/s downlink and 1.5 Gbit/s uplink optical wireless transmission at indoor distances (1.5m)," in *Proc. Eur. Conf. Opt. Commun.*, Sep. 2014, pp. 1–3.

[21] P. Butala, J. Chau, and T. Little, "Metameric modulation for diffuse visible light communications with constant ambient lighting," in *Proc. Int. Workshop Opt. Wireless Commun.*, Oct. 2012, pp. 1–3.

[22] R. Drost and B. Sadler, "Constellation design for channel precompensation in multi-wavelength visible light communications," *IEEE Trans. Commun.*, vol. 62, no. 6, pp. 1995–2005, Jun. 2014.

[23] Y. Ohno, "CIE fundamentals for color measurements," in *Proc. IS&T NIP16*, Oct. 2000, vol. 2000, no. 2, pp. 540–545.

[24] *Colour Rendering (tc 1-33 Closing Remarks)*(Publication 135/2). Vienna, Austria: CIE Central.

[25] K.-I. Ahn and J. Kwon, "Color intensity modulation for multicolored visible light communications," *IEEE Photon. Technol. Lett.*, vol. 24, no. 24, pp. 2254–2257, Dec. 2012.

[26] M. Beko and R. Dinis, "Designing good multi-dimensional constellations," *IEEE Wireless Commun. Lett.*, vol. 3, no. 1, pp. 221–224, Jun. 2012.

[27] M. Grant and S. Boyd, "CVX: MATLAB software for disciplined convex programming, version 2.1," Mar. 2014. [Online]. Available: http://cvxr.com/cvx.

[28] M. Grant and S. Boyd, "Graph implementations for nonsmooth convex programs," in *Recent Advances in Learning and Control*, V. Blondel, S. Boyd, and H. Kimura, Eds. NEw York, Ny, USA: Springer-Verlag, 2008, pp. 95–110.

[29] Lumileds, LUXEON C Color Line Product Datasheet. Jun. 2016. [Online]. Available: http://www.lumileds.com/uploads/571/DS144-pdf.

[30] Hamamatsu Inc., Photodiode S5343. Apr. 2004. [Online]. Available: http://www.datasheet.com/hamamatsu/s5343.htm.

[31] Semrock Inc., 615/20nm single-band bandpass filter. Mar., 2016. [Online]. Available: https://www.semrock.com/FilterDetails.aspx?id=FF02-615/20-25

[32] Semrock Inc., 538/40nm single-band bandpass filter. Mar. 2016. [Online]. Available: https://www.semrock.com/FilterDetails.aspx?id=FF01-538/40-25.

[33] Semrock Inc., 475/50nm single-band bandpass filter. Mar. 2016. [Online]. Available: https://www.semrock.com/FilterDetails.aspx?id=FF02-475/50-25.

[34] Semrock Inc., 590/20nm single-band bandpass filter. Mar. 2016. [Online]. Available: https://www.semrock.com/FilterDetails.aspx?id=FF01-590/20-25.

[35] Philips, Philips LED Bulb. Aug. 2015. [Online]. Available: https://www.download.p4c.philips.com/files/0/046677455811/04667745581 1_pss_aenus.pdf.

[36] J. Thorpe, "Low-density parity-check (LDPC) codes constructed from protographs," Jet Propulsion Lab., Pasadena, CA, USA, IPN Progr. Rep., vol. 42-154, pp. 1–7, Aug. 2003.

[37] *Draft IEEE Standard for Local and Metropolitan Area Networks Part 16: Air Interface for Fixed and Mobile Broadband Wireless Access Systems Amendment for Physical and Medium Access Control Layers for Combined Fixed and Mobile Operation in Licensed Bands*, IEEE P802.16e/D12, Oct. 2005.

[38] H. Xiao and A. H. Banihashemi, "Improved progressive-edge-growth (PEG) construction of irregular LDPC codes," *IEEE Commun. Lett.*, vol. 8, no. 12, pp. 715–717, Dec. 2004.

[39] F. Schreckenbach, N. Görtz, J. Hagenauer, and G. Bauch, "Optimization of symbol mappings for bit-interleaved coded modulation with iterative decoding," *IEEE Commun. Lett.*, vol. 7, no. 12, pp. 593–595, Dec. 2003.

[40] R. Roberts, S. Rajagopal, and S.-K. Lim, "IEEE 802.15.7 physical layer summary," in *Proc. Globecom Workshops*, Dec. 2011, pp. 772–776.

[41] *IEEE Standard for Local and Metropolitan Area Networkscpart 15.7: Short-Range Wireless Optical Communication Using Visible Light*, IEEE Standard 802.15.7-2011, Jun. 2011.

[42] X. Huang, J. Shi, J. Li, Y. Wang, and N. Chi, "A Gb/s VLC transmission using hardware preequalization circuit," *IEEE Photon. Technol. Lett.*, vol. 27, no. 18, pp. 1915–1918, Sep. 2015.

Xiao Liang (S'12–M'13) received the B.Sc., M.S., and Ph.D. degrees in communication and information engineering all from Southeast University, Nanjing, China, in 2000, 2005, and 2013, respectively.

He is currently a Lecturer with National Mobile Communications Research Laboratory, Southeast University, Nanjing, China. His research interests include signal processing for communications and wireless networking.

Ming Yuan received the B.Sc. degree from the Southeast University, Nanjing, China, in 2014, where he is currently working toward the Master's degree with the National Mobile Communication Research Laboratory, Southeast University. His research interest includes the high-speed visible light communications.

Jiaheng Wang (M'10–SM'14) received the Ph.D. degree in electronic and computer engineering from the Hong Kong University of Science and Technology, Kowloon, Hong Kong, in 2010, and the B.E. and M.S. degrees from the Southeast University, Nanjing, China, in 2001 and 2006, respectively.

He is a Full Professor at the National Mobile Communications Research Laboratory, Southeast University, Nanjing, China. From 2010 to 2011, he was with the Signal Processing Laboratory, KTH Royal Institute of Technology, Stockholm, Sweden. He also held visiting positions at the Friedrich Alexander University Erlangen-Nürnberg, Nürnberg, Germany, and the University of Macau, Macau. He has published more than 80 articles on international journals and conferences. His research interests include mainly optimization in communication systems and wireless networks.

Dr. Wang serves as an Associate Editor of the IEEE SIGNAL PROCESSING LETTERS. He received the Humboldt Fellowship for Experienced Researchers, and the Best Paper Award in WCSP 2014.

Zhi Ding (S'88–M'90–SM'95–F'03) received the Ph.D. degree in electrical engineering from Cornell University, Ithaca, NY, USA, in 1990. He is a Professor of electrical and computer engineering at the University of California, Davis, CA, USA.

From 1990 to 2000, he was a faculty member of Auburn University and later, University of Iowa. He has held visiting positions in Australian National University, Hong Kong University of Science and Technology, NASA Lewis Research Center, and USAF Wright Laboratory. He has active collaboration with researchers from several countries including Australia, China, Japan, Canada, Taiwan, Korea, Singapore, and Hong Kong. He is a coauthor of the text: *Modern Digital and Analog Communication Systems*, 4th ed., (Oxford Univ. Press, 2009).

Dr. Ding is serving on technical programs of several workshops and conferences. He was an Associate Editor of the IEEE TRANSACTIONS ON SIGNAL PROCESSING from 1994 to 1997, 2001 to 2004, and an Associate Editor of the IEEE SIGNAL PROCESSING LETTERS from 2002 to 2005. He was a member of technical committee on Statistical Signal and Array Processing and member of technical committee on Signal Processing for Communications (1994–2003). He was the General Chair of the 2016 IEEE International Conference on Acoustics, Speech, and Signal Processing and the Technical Program Chair of the 2006 IEEE Globecom. He was also an IEEE Distinguished Lecturer (Circuits and Systems Society, 2004–06, Communications Society, 2008–09). He served as the IEEE Transactions on Wireless Communications Steering Committee Member (2007–2009) and its Chair (2009–2010).

Ming Jiang (S'06–M'07) received the B.Sc., M.S., and Ph.D. degrees in communication and information engineering all from Southeast University, Nanjing, China, in 1998, 2003, and 2007, respectively.

He is currently an Associate Professor with National Mobile Communications Research Laboratory, Southeast University, Nanjing, China. His research interests include coding and modulation technology.

Chunming Zhao received the B.Sc. and M.S. degrees from Nanjing Institute of Posts and Telecommunications, Nanjing, China, in 1982 and 1984, respectively. In 1993, he received the Ph.D. degree from the Department of Electrical and Electronic Engineering, University of Kaiserslautern, Kaiserslautern, Germany. He has been a Postdoctoral Researcher at National Mobile Communications Research Laboratory, Southeast University, Nanjing, China, where he is currently a Professor and the Vice Director of the Laboratory. He has managed several key projects of Chinese Communications High Tech. Program and was awarded as "excellent researcher" form Ministry of Science and Technology, China. His research interests include communication theory, coding/decoding, mobile communications, and VLSI design.